A Fully Integrated Nanosystem of Semiconductor Nanowires for Direct Solar Water Splitting

Chong Liu[1,3]†, *Jinyao Tang*[1]†, *Hao Ming Chen*[1], *Bin Liu*[1], *Peidong Yang*[1,2,3*]

[1] Department of Chemistry, and [2] Department of Materials Science and Engineering, University of California, Berkeley, California 94720,

[3]Materials Sciences Division, Lawrence Berkeley National Laboratory, Berkeley, California 94720

† These authors contributed equally to this work

* To whom correspondence should be addressed. Email: p_yang@berkeley.edu

Table of Contents:

I. Materials and Methods: synthesis, optimization, and characterization of Si/TiO_2 nano-tree heterostructures

1. Synthesis of silicon nanowire array substrates
2. Synthesis of titanium oxide nanowire array substrates
3. Iridium oxide (IrO_x) nanoparticles for oxygen evolution
4. Electroless deposition of platinum (Pt) for hydrogen evolution
5. Synthesis of the Si/TiO_2 nano-tree heterostructures
6. Photocatalytic characterization methods
7. Calculation of the energy conversion efficiency and faradic efficiency
8. Estimation of the relative photoactivity of the Si/TiO_2 nano-tree heterostructures

II. Optimization of the Si and TiO_2 nanowire photoelectrodes and the effect of the method used for loading cocatalysts

III. Charge transport at the Si/TiO_2 interface

IV. Control experiments for the water splitting of nano-tree heterostructures

V. Comparison of the water-splitting performance of nano-tree heterostructures with other approaches

VI. General applicability of the nanoscale tree-shape heterostructure design for the "Z-scheme" processes in solar-to-fuel conversion

I. Experimental methods for the synthesis, optimization, and characterization of Si/TiO_2 nano-tree heterostructures

1. Fabrication of the silicon nanowire array substrates

Silicon (Si) nanowire arrays were fabricated using reactive-ion etching of patterned single-crystalline Si wafers. P-type boron-doped 4'' Si wafers (<100> oriented, 0.1~0.2 Ω•cm) were first patterned with a photoresist dot array using a standard photolithography stepper. Then the wafer underwent inductive-coupled plasma deep reactive-ion etching (Surface Technology Systems, Inc.) to produce nanowire arrays with uniform diameter ~850 nm and length ~30 μm. After removing the residual photoresist by an O_2 plasma, 50 nm of dry thermal oxide was grown on the nanowires at 1050 °C for 40 min. After a 5:1 buffered HF etch and critical point drying (Tousimis, Inc.), Si nanowire arrays with wires whose diameters were about 800 nm were obtained.

To optimize the Si nanowire photocathode, a thin, highly doped n^+ layer was formed on the surface of the Si nanowires for better photovoltage output, similar to the approach reported in reference 24. A Si handle wafer was spin-coated with arsenic-containing spin-on dopant (SOD) (Filmtronics, Inc.) at 3000 rpm for 1 min and then baked at 150 °C on a hotplate for 30 min. This handle wafer was used as a local arsenic source for proximity doping to form the n^+ layer on the silicon nanowire surface. The HF-vapor treated Si nanowire substrate was then placed on the SOD-coated handle wafer and subjected to rapid thermal annealing at 900-1000 °C for 1-3 min in argon. The formation of an n^+ layer on the nanowire's surface was confirmed when the onset

potential of the silicon nanowire photocathode shifted cathodically 150-250 mV as compared to that of the untreated nanowire photocathode; a similar result was reported in reference 24.

2. Synthesis of the titanium oxide nanowire array substrates

Titanium oxide (TiO_2) nanowires were synthesized via hydrothermal methods according to reference 23. In a typical synthesis, 0.167 g of titanium tetraisopropoxide (Sigma-Aldrich) was mixed with 10 ml of 6 M hydrochloric acid (Sigma-Aldrich) and poured into a 40 ml Teflon container. A fluorine-doped tin oxide (FTO) substrate was also introduced into the container and hydrothermally treated at 100-200 °C for several hours. After cooling, an array of single-crystalline rutile TiO_2 nanowires had grown on the FTO substrate.

3. Iridium oxide (IrO_x) nanoparticles for oxygen evolution

IrO_x nanoparticles were loaded onto the TiO_2 nanowires to increase the photocurrent's fill factor in an acidic environment. The synthesis of IrO_x used a modification of the recipe reported before (Y. Zhao, *et. al*., *J. Phys. Chem. Lett*., **2011**, *2*, 402-406). In a typical synthesis, 30 ml of 1 mM sodium hexachloroiridate(IV) hexahydrate (Sigma-Aldrich) solution was mixed with 0.3 ml of 0.1 M potassium hydroxide (Sigma-Aldrich), and heated on a 90 °C hotplate. The color of the solution evolved from brown to transparent and then gradually darkened to purple. The heating was stopped when the color was transparent with tinted purplish-blue. The resultant solution was transparent and stable at 4 °C for months without precipitation. IrO_x nanoparticles were loaded

onto the TiO_2 nanowires by soaking the nanowires in five-times diluted IrO_x solution for several hours, during which the IrO_x nanoparticles adsorbed onto the surface of the nanowires.

4. Electroless deposition of platinum (Pt) for hydrogen evolution

Platinum was electrolessly deposited onto the surface of the Si nanowires as the hydrogen evolution cocatalyst using a method similar to the one reported in reference 24. The Si nanowire array was immersed in a solution containing 0.5 M hydrofluoric acid (Sigma-Aldrich) and 0.5 mM hexachloroplatinic acid hexahydrate (Sigma-Aldrich) for 2 min and then rinsed with deionized water. This process was cycled for two to three times to achieve an optimal response from the photocathode. Because the deposition of platinum consumes Si as a reductant, the platinum deposited on only the Si surface in the case of the nano-tree heterostructures. This minimized the possible back-reactions induced by platinum on the TiO2 surface, as mentioned in reference 29.

5. Synthesis of the Si/TiO_2 nano-tree heterostructures

The synthesis of the Si/TiO_2 heterostructures combined the synthesis of the Si and TiO_2 nanowires, in which all components were compatible and retained their photoactivity. A detailed synthetic scheme is displayed in Supplementary Figure 1. After fabrication of the silicon nanowire array as described above, a conformal polymer coating of parylene-N was applied at room temperature (Specialty Coating Systems, Inc.) to embed the n^+/p Si nanowire array. The polymer-coated array was then treated with an O_2 plasma to expose the top half of the Si

nanowires. An aqueous solution of potassium hydroxide (20 wt%) was applied for 1-2 min to remove the n^+ layer on the top half of Si nanowires, resulting in asymmetric nanowire structures with p-type tops and n^+/p core-shell bottoms. A parylene coating was applied again to embed the nanowires in polymer and then etched by an O_2 plasma. To avoid reducing the shunt resistance between the n^+ Si layer and the ohmic contact formed later between the Si and TiO_2, a gap was left between the first and second parylene etches. Then 5-10 nm of platinum was sputtered onto the substrate (Edwards, Inc.) and a seed layer for TiO_2 nanowire growth was deposited either by atomic layer deposition or by vacuum sputtering before being treated with rapid thermal annealing at 400 °C for 15 sec in argon. After removal of the residual parylene polymer by either an O_2 plasma or annealing in O_2 at 450 °C for 30 min, the nanowire substrate was then used for hydrothermal TiO_2 nanowire synthesis to produce the Si/TiO_2 nano-tree heterostructures after a subsequent 450 °C anneal for 30 min.

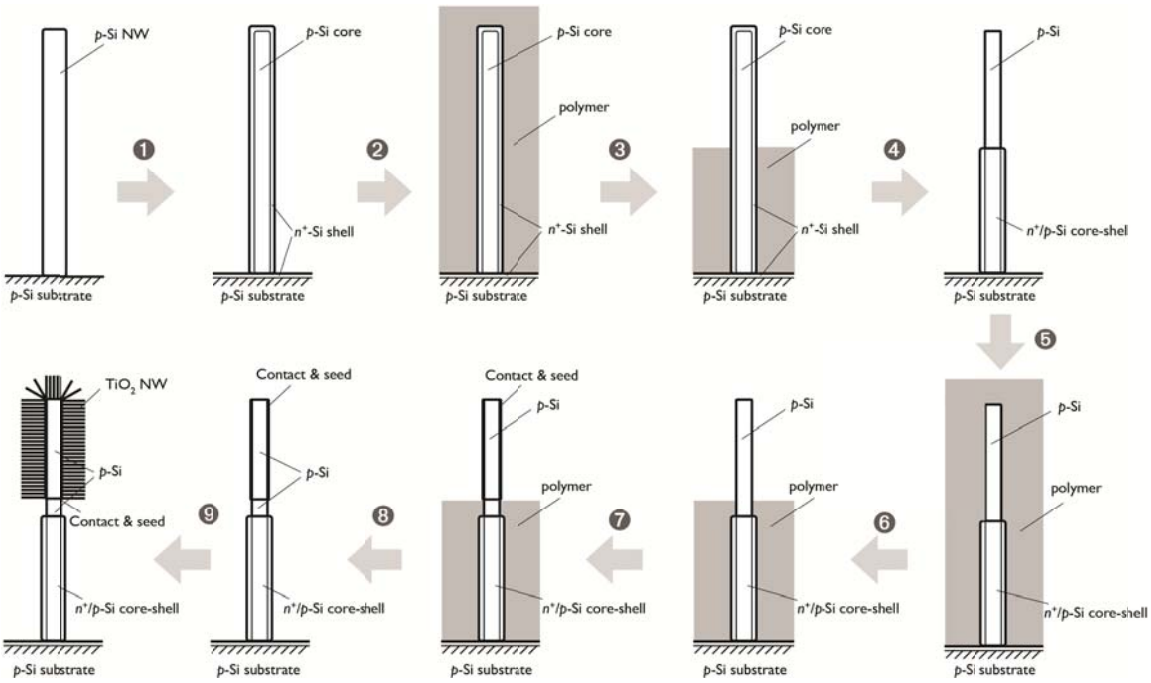

Supplementary Figure 1 Synthetic scheme for the Si/TiO_2 nano-tree heterostructures, starting from a p-type Si nanowire array. A detailed description of the procedure is described in the supplementary methods section.

6. Photocatalytic characterization methods

For optimization of the individual components of the nano-tree heterostructures, photoelectrochemical measurements of individual electrodes were performed using a Gamry reference 600 potentiostat. All measurements were performed under an inert helium environment and in a 0.5 M sulfuric acid electrolyte (pH = 0.52). Ag/AgCl in 3 M NaCl (ALS, Corp.) was used as the reference electrode when needed, and all voltages reported were calculated *versus* the reversible hydrogen electrode (RHE) using the following equation:

$$V \text{ vs RHE (volt)} = \text{V vs Ag/AgCl (volt)} + 0.234 \text{ (volt)}$$

The light source used for simulated sunlight in this report was a 300-Watt xenon lamp equipped with an air mass 1.5G filter (Newport). Before each measurement, a calibrated silicon

photodiode determined the light intensity at the position of the electrode being measured. All photoresponses were measured right after the cocatalyst loading procedures described above.

The *J-V* photocurrent data for individual photoelectrodes were measured using a standard three-electrode setup under simulated one-sun illumination, with a scan rate of 10 mV/sec. The dark currents were orders of magnitude lower than photocurrent in all cases within the voltage ranges measured.

The short-circuit measurements of externally wired Si and TiO_2 nanowire electrodes were performed using a two-electrode setup, in which the potentiostat remained short-circuited and behaved as an ammeter. The two photoelectrodes were in the same reaction chamber and placed side by side in the region of light exposure.

To measure the amount of gas evolved in the photoelectrochemical process, the system was designed as a batch reactor in a helium environment. A bubbler purged the electrolyte in the reactor to bring the evolved gases into a gas chromatograph for analysis. After that, the gas was fed back into the reactor via a recirculation pump. The gas chromatograph (SRI Instrument, Inc.) was equipped with a molecular sieve 13X packed column and a helium ionization detector. Before each reaction the system was calibrated with H_2 and O_2 gases of known concentration.

In order to test the photoactivity of the Si/TiO_2 nano-tree heterostructures, a similar system as the one used for externally wired electrodes was applied, except that there were no ports for the electrodes. After loading of the cocatalysts, Si/TiO_2 nanowire heterostructures were removed

from the substrate and dispersed in electrolyte. The dispersion was loaded into the reactor and exposed to simulated sunlight after constant gas purging to remove O_2 in the reactor. After every 90 min while the photocatalytic reaction continued, the system was purged with helium to remove evolved gas product.

7. Calculation of the energy conversion efficiency and faradic efficiency

The energy conversion efficiency of the solar-driven water splitting η was calculated based on the measured amount of evolved H_2 gas, using the following equation,

$$\eta = \frac{2 \times 1.23(V) \times N_{H2}(mol) \times 96485(C \cdot mol^{-1})}{I(W \cdot cm^{-2}) \times A(cm^2) \times t(\sec)} \times 100\%$$

in which N_{H2} is the amount of evolved H_2 gas, I is the light intensity, A is the projected area of light exposure, and t is the elapsed time of reaction. For all measurements the photoactivities of the first fifteen minutes were used for above calculation. For the calculation of the faradic efficiency of the water-splitting evolution $\eta_{faradic}$ in the configuration of short-circuited electrodes, the following equation was applied,

$$\eta_{faradic} = \frac{2 \times N_{H2}(mol) \times 96485(C \cdot mol^{-1})}{Q(C)} \times 100\%$$

in which Q is the total amount of charge passed through the external circuit during the same time period of time as the measurement of evolved H_2 gas.

8. Estimation of the relative photoactivity of the Si/TiO_2 nano-tree heterostructures

The estimation of the relative photo-activity of the Si/TiO_2 nano-tree heterostructures was based on the *J-V* photocurrent data shown in Figure 2b. Mathematically, the *J-V* data of the Si nanowire photocathode and TiO_2 nanowire photoanode are expressed as voltage (*versus* RHE) dependent function, $J_{Si}(V)$ and $J_{TiO2}(V)$. For a certain percentage by length of TiO_2 on the nanotree heterostructre *c* ($0 < c < 1$), the photocurrent $J_0(c)$ that flows through the connection between the two electrodes would have following form because of the current-matching requirement of the Z-scheme (see reference 8),

$$J_0(c) = (1-c)J_{Si}(V = V_c(c)) = cJ_{TiO2}(V = V_c(c))$$

in which $V_c(c)$ is the *c*-dependent voltage where $J_{Si}(V)$ and $J_{TiO2}(V)$ intersect. For different values of *c*, the $V_c(c)$ was calculated. Subsequently the photocurrent of the short-circuited electrodes $J_0(c)$ was obtained, enabling estimation of the photoactivity of the nano-tree heterostructures. Because of possible extra loss mechanisms existing in the Si/TiO_2 nano-tree heterostructures (e.g. poor light absorption or chemical back reactions), only the normalized relative photoactivity is plotted in Figure 4b, which assumes that the photo-activity is degraded by a constant factor as compared to that of the linked electrodes.

II. Optimization of the Si and TiO_2 nanowire photoelectrodes and the effect of the method used for loading cocatalysts

To achieve optimized performance of the Si/TiO_2 nano-tree heterostructures, it is important to optimize the individual components of the integrated system first. As known in the literature, Si photocathodes (reference 24) and TiO_2 photoanodes (reference 28) function in aqueous solutions of different pH. Si photocathodes work best in acidic environments because of the instability of Si in basic solution and the decreased catalytic activity of the H_2-generating cocatalyst. On the other hand, although TiO_2 is still photoactive in acidic solution, in basic solution it has higher faradic efficiency and enough catalytic activity to drive water oxidation without any cocatalyst. In this work, Si was loaded with Pt nanoparticles via the electroless deposition method (Supplementary Figure 2a), while the TiO_2 nanowire photoanode was modified with IrO_x nanoparticles to improve its photoactivity in acidic electrolyte (Supplementary Figure 2b). The loading of IrO_x nanoparticles did not change the onset potential of the TiO_2 photocurrent, but it did improve its fill-factor by increasing the surface catalytic activity of oxygen evolution. Moreover, the electroless deposition method of the Pt cocatalyst prevents any Pt loading on TiO_2 surface in the nano-tree heterostructures, thus minimizing the possible induced back-reactions (reference 27). The IrO_x adsorbed on all the materials, but it did not induce any negative effects on the Si nanowire photocathode (Supplementary Figure 3). Therefore the loading of both Pt and IrO_x cocatalysts is compatible with the nano-tree heterostructures.

To further confirm the existence of co-catalysts, high-resolution transmission electron microscope (HRTEM) and scanning transmission electron microscope (STEM) characterizations

were carried out (Supplementary Figure S4). Owing to the large diameter of Si wires, HRTEM imaging for the photocathode is not fruitful. On the photoanode side, both HRTEM and STEM images reveal a uniform coating of IrO_x co-catalysts in the form of 1~2 nm nanoparticles. Energy dispersive X-ray spectroscopy (EDS) mapping of Ir element also confirmed a uniform co-catalyst loading. The absence of Pt signal on the TiO_2 surface confirmed the selective deposition of Pt on the photocathode surface.

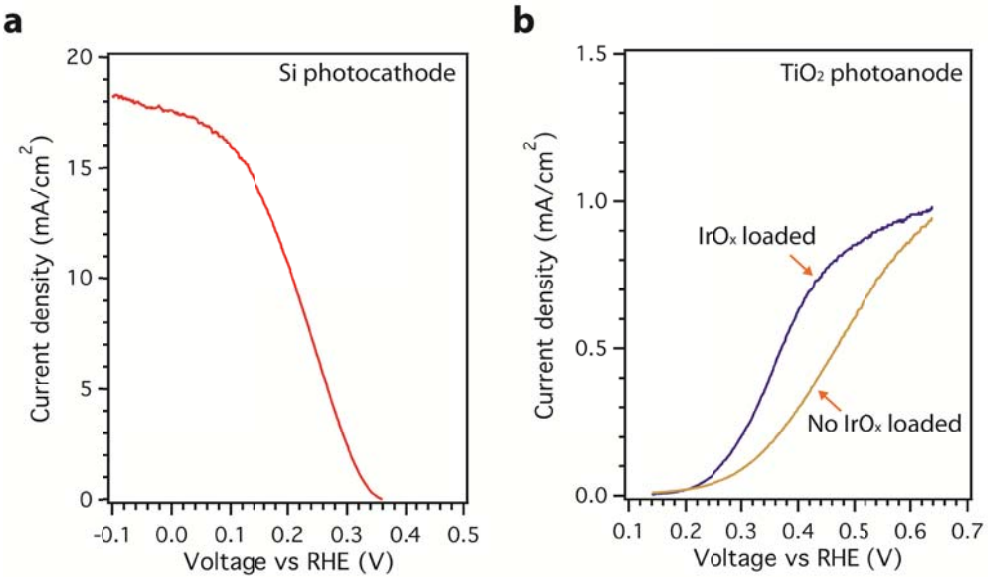

Supplementary Figure 2 Optimized photoelectrochemical performance of a Si nanowire photocathode (**a**) and a TiO_2 nanowire photoanode (**b**) in 0.5 M sulfuric acid electrolyte. The absolute values of both photocurrents were displayed. **a** is the same curve as in Figure 2b, only plotted over a wider voltage range. Both figures are the median performance from more than six batches. Loading IrO_x nanoparticles increases the fill-factor of the photocurrent of the TiO_2 nanowire photoanode, as illustrated in **b**.

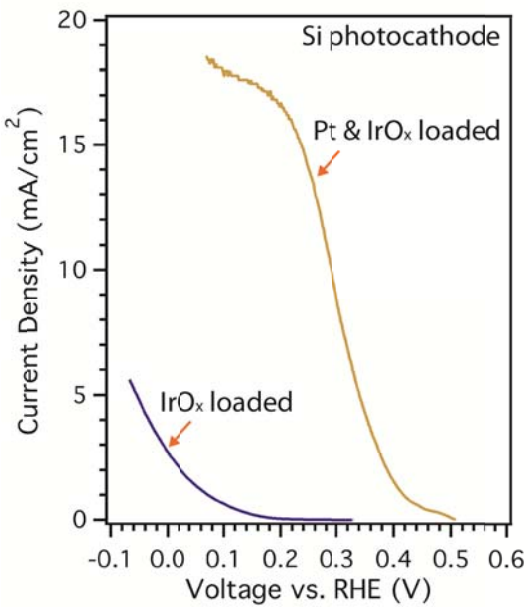

Supplementary Figure 3 The effect of oxygen-generating IrO_x nanoparticles on the Si photocathode. During loading of the cocatalyst, IrO_x nanoparticles adsorb indiscriminately on all surfaces, so their effect on the Si nanowire photocathode needs to be addressed. As shown in the figure, IrO_x nanoparticles themselves are not catalytic for hydrogen evolution, nor do they hinder the catalytic properties of Pt. Although Pt is reported to promote the back-reaction on TiO_2 (reference 27), our electroless deposition method requires the consumption of Si and therefore prevents deposition of Pt onto the TiO_2 surface.

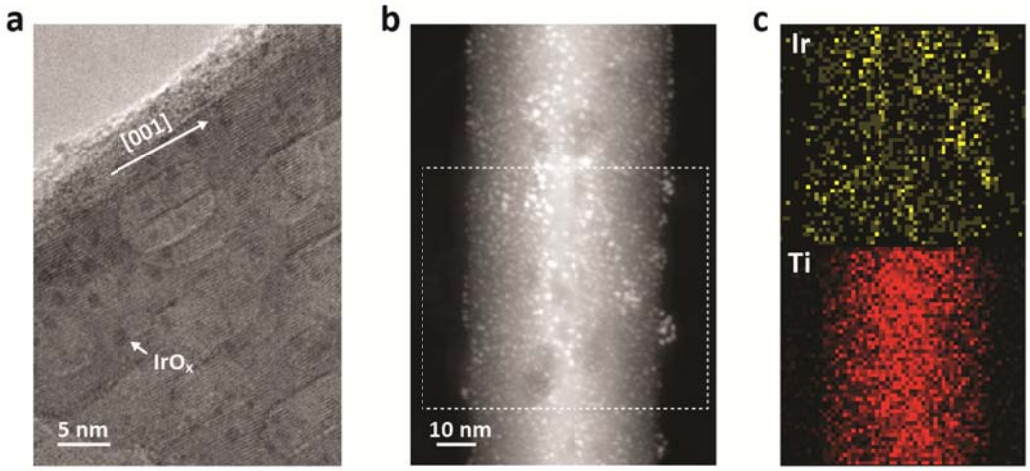

Supplementary Figure 4 The loading of IrO_x co-catalyst was investigated on the TiO_2 portion of the nano-tree heterostructure. From high-resolution transmission electron microscope (HRTEM) image (**a**), IrO_x nanoparticles of 1~2 nm diameter are observable on the nanowire surface. The uniformity of IrO_x loading on TiO_2 surface is further confirmed with scanning transition electron microscope (STEM) images (**b**). Additional energy dispersive X-ray spectroscopy (EDS) mapping in the highlighted area in (**b**) confirmed that the nanoparticles contains iridium element (**c**), and platinum signal is absent.

III. Charge transport at the Si/TiO_2 interface.

To finish up the relay of charge carriers between the two semiconductors in the nano-tree heterostructures' "Z-scheme", a metallic contact was required for charge transport at the Si/TiO_2 interface. As noted in the experimental methods section, a silicide-based contact was applied to the nano-tree heterostructure. By comparing the photocurrent behavior of a TiO_2 nanowire array grown on an FTO substrate with that of TiO2 nanowires grown on a p-type Si nanowire array, it is clear that the contact to the Si nanowires is not ideal; a shift of about 50 mV in photovoltage was observed (Supplementary Figure 5). Improving the contact between Si/TiO_2 interface remains as an ongoing effort.

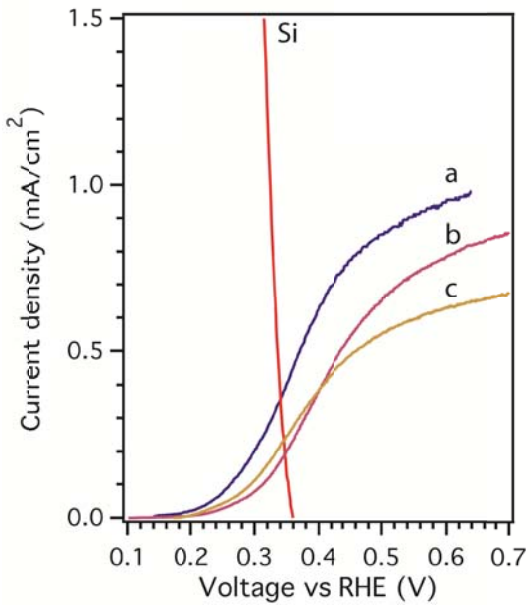

Supplementary Figure 5 Effect of the ohmic contact at the TiO_2 and Si interface. The photoanodic response of TiO_2 nanowires grown on an FTO substrate (**a**), planar p-type Si substrate (**b**), p-type Si nanowire array (**c**). Curve **a** is the same as shown in Figure 2a, and for comparison the Si nanowire photocathode photocurrent curve is shown as well. With a loss of about 50 mV in photovoltage, an ohmic contact at the Si and TiO_2 interface is realized.

IV. Control experiments for the water splitting using nano-tree heterostructures.

Several control experiments were performed to verify that the observed water splitting originated from the nano-tree heterostructures. As shown in Supplementary Figure 6, there was no significant water splitting from dispersions of pure Si nanowires, pure TiO_2 nanowires, or the mixture of Si and TiO_2 nanowires. The former two controls confirmed that the individual components of the nano-tree heterostructures were not capable of realizing complete water splitting individually; and the latter control suggested that no water splitting was observable in the absence of a well-defined local contact. Based on these observations, the solar-driven water splitting arose solely from the nano-tree heterostructure, and the importance of the local contact was illustrated.

Another important control experiment is the comparison of photocatalytic performance between the integrated nano-tree structure and an asymmetric core-shell nanostructure that a thin film TiO_2 is deposited onto part of Si nanowire (Supplementary Figure 7). The latter structure design contains the same feature of "Z-scheme" process, but the physical properties of materials are not considered for optimal performance, particularly the absence of large surface area for TiO_2 photoanode. Supplementary Figure 7 shows that the photocatalytic performance of this non-optimal design. The weight-normalized performance is about 90 μmol/hr H_2 for 1 gram of material, much lower than the value of nanotree structure (about 875 μmol/hr H_2 for 1 gram of material). Here the necessity of rational nanostructure/interface design based on the physical properties of materials is illustrated.

As shown in Figure 4b, nano-tree heterostructures with varying percentages of TiO_2 were tested to optimize performance. The corresponding scanning electron microscope (SEM) images of the tested samples are shown in Supplementary Figure 8.

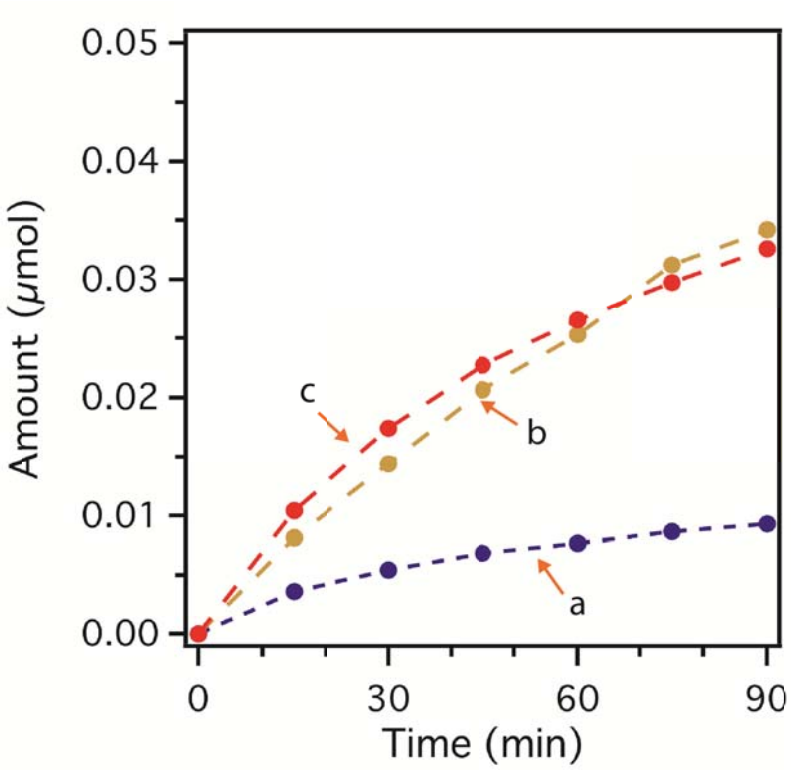

Supplementary Figure 6 Control experiments for the nano-tree heterostructures. The measured amounts of evolved H_2 gas for Si nanowires (**a**), TiO_2 nanowires (**b**), and a random mixture of Si and TiO_2 nanowires without well-defined contacts (**c**). The order-of-magnitude-lower gas evolution rate proves the functionality of the nanotree heterostructures. The amount of evolved O_2 gas is not shown because the signal level was on the same order of magnitude as the O_2 leakage of the reactor.

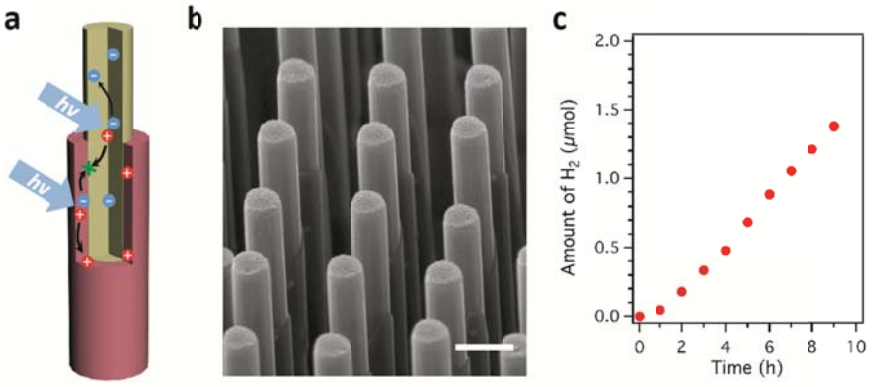

Supplementary Figure 7 Control experiment for the non-optimal integrated nanostructure. A schematic design is displayed in (**a**), in which one Si nanowire photocathode (yellow) is partially coated with a thin-film version of TiO_2 photoanode (red). The nanostructure is characterized using SEM (**b**), and the photocatalytic performance of water splitting is measured (**c**). The gas evolution rate is much lower than that displayed in Figure 4a, clearly demonstrating the advantage of nanoscale-tree design reported here. The amount of evolved O_2 gas is not shown since the data is not conclusive. The scale bar is 1 μm.

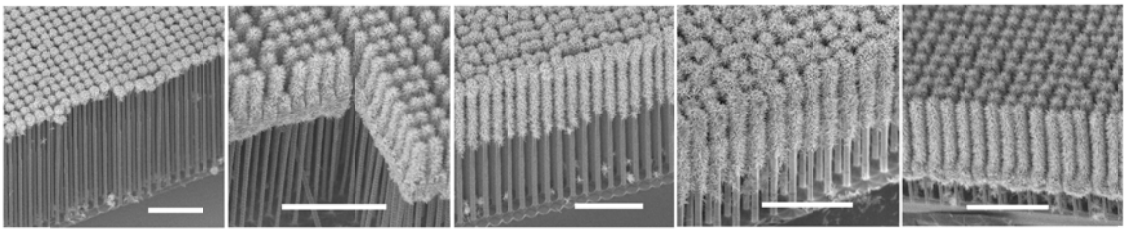

Supplementary Figure 8 Si/TiO_2 nano-tree heterostructures with varying percentages of TiO_2, which correspond to the water-splitting photo-activity measurements shown in Figure 4b. The scale bars are all 10 μm.

V. Comparison of the water-splitting performance of the nano-tree heterostructures with other approaches.

The following table compares the photoactivity of several different approaches to water splitting reported in the literature. Here we compare the weight-normalized water-splitting performance from both the macroscopic electrodes and powder photocatalyst approaches by analyzing our own experiments and other results reported before. It should be noted that the reports in the literature use different light sources, so the comparison can only be made in a qualitative manner. As shown in the table, our nano-tree heterostructures have higher weight-normalized performance than the Si-TiO_2 linked electrode approach when normalized under the same light intensity. Compared with other reported powder photocatalyst approaches, the nano-tree heterostructures also show a higher value despite the variation in light sources.

Supplementary Table 1: Comparison of the weight-normalized performance of different approaches.

Photocatalysts system	Type of approach	Weight-normalized performance ($\mu mol \bullet hr^{-1} \bullet g^{-1}$)	Light source
Si/TiO_2 nano-tree[a]	Integrated nanosystem	875	300W Xenon lamp AM 1.5G 150mW/cm^2
$Si\text{-}TiO_2$ linked electrode[a]	Electrode	~1810[b] ~32[c]	300W Xenon lamp AM 1.5G 300mW/cm^2
$Ru/SrTiO_3$:Rh + $BiVO_4$[d]	Powder	200	300W Xenon lamp > 420 nm
$Ru/SrTiO_3$:Rh + TiO_2[d]	Powder	335	300W Xenon lamp > 300 nm
GaN/ZnO[e]	Powder	1000	450W Hg lamp 2M $NaNO_2$ filter

[a] Data reported in the current work.

[b] Calculated based on the weight of the active materials, i.e. the weight of the Si nanowire arrays and the TiO_2 nanowires. It should be noted that for the macroscopic electrode approach, this value is an upper limit to weight-normalized performance because other materials, for example the underlying Si substrates, are needed for the electrode devices to function.

[c] Calculated based on the overall device weight, which includes the underlying Si substrate and the minimal FTO glass substrate needed for TiO_2 nanowire growth. This value sets a lower limit for the weight-normalized performance in practical applications.

[d] Calculated from: Y. Sasaki, *et. al*., *J. Phys. Chem. C*, **2009**, *113*, 17536-17542, whose result is also cited in reference 18.

[e] Calculated from D. Lu, *et. al*., *Nature*, **2006**, *440*, 295, whose result is also cited in reference 19.

VI. General applicability of the nanoscale tree-shape heterostructure design for the "Z-scheme" processes in solar-to-fuel conversion.

As discussed in the manuscript, the tree shaped nanostructure is designed based on careful consideration of the electrical and optical properties of both Si and TiO_2 materials. Because of the vastly different properties of the two materials (Si and TiO_2), a tree shaped nanostructure would serve best for the integrated nanosystem. Particularly, TiO_2 needs large surface area and smaller diameters to facilitate the kinetic-limited oxidation reaction and improve the charge collection efficiency of photo-generated carriers, whereas Si possesses better charge collection efficiency and ultra-high surface area is really not desirable in order to minimize the recombination at surface states.

This discrepancy in length scale between photocathode and photoanode is general for many material and catalytic systems available at this moment. Fundamentally when we consider many semiconductor materials for solar-to-fuel conversion, the conduction band is more likely to have a more delocalized feature therefore a smaller effective mass; while the valence band usually is more localized, for example the *p* orbitals of oxygen and nitrogen in many photoanode materials, therefore has a larger effective mass. This means that the photo-excited electrons in the conduction band of photocathode, for example Si, InP/GaP, and Cu_2O, are typically more mobile, while usually the photo-generated holes in the valence band of photoanode (TiO_2, WO_3, Fe_2O_3, etc.) have smaller mobility. This general trend leads to a demand of smaller feature size for photoanode materials to achieve high charge collection efficiency, as compared to that of photocathode materials. Moreover kinetically it is well-known that the overpotential issue is much more significant for water oxidation compared to proton reduction, fundamentally because

the 4-electron transfer of water oxidation comprises of more elementary steps than that of 2-electron transfer in proton reduction. Hence a larger surface area for water oxidation process would be more desirable than for proton reduction, in order to reduce reaction overpotential. The differences in material properties and reaction kinetics between photoanode and photocathode lead to different requirements in the length scale and surface area of nanomaterials for optimal performance, which implies that a tree-shaped architecture would be one of the ideal designs.